ACCSCIENCE PUBLISHING

International Journal of Bioprinting

RESEARCH ARTICLE

Construction and application of a novel 3D bioprinting-based *in vitro* nasopharyngeal carcinoma model for drug screening and mechanistic research

Haijie Zhao[1,2†], Hang Sun[3†], Huayu Yang[1*], and Yilei Mao[1*]

[1]Department of Liver Surgery, Peking Union Medical College Hospital, Chinese Academy of Medical Sciences & Peking Union Medical College, Beijing, China

[2]Eight-year MD Program, Chinese Academy of Medical Sciences & Peking Union Medical College, Beijing, China

[3]Department of General Surgery, Beijing Friendship Hospital, Capital Medical University, National Clinical Research Center for Digestive Diseases, Beijing, China

Abstract

Nasopharyngeal carcinoma (NPC) is a prominent head and neck malignancy, yet the mechanisms underlying its occurrence, progression, recurrence, metastasis, drug resistance, and radiation resistance have not been fully understood. This knowledge gap is partly due to the lack of preclinical NPC models for research. Compared to traditional 2D cell cultures, 3D bioprinting (3DP) offers significant advantages in replicating the tumor microenvironment. However, no studies to date have used 3DP technology to model NPC. In this study, we used extrusion-based 3DP to develop a new preclinical NPC model (3DP-HK1) using the emerging bio-ink gelatin methacryloyl. The model successfully demonstrated the ability to sustain long-term tumor cell activity. Immunohistochemistry and immunofluorescence analyses demonstrated that 3DP-HK1 largely retained the histopathological features and tumor-related protein expression of NPC. In addition, we conducted a wound healing experiment, which indicated that tumor cells in 3DP-HK1 have stronger migration ability than 2D-cultured cells (2D-HK1), highlighting differences in cellular phenotype. The different responses of 3DP-HK1 and 2D-HK1 to various anti-tumor drugs and radiation reflect the advantages of 3DP-HK1 for preclinical drug screening and exploring mechanisms of radiotherapy in NPC. Transcriptome sequencing revealed that 3DP-HK1 has a distinct gene expression profile compared to 2D-HK1, with significantly upregulated expression of malignant genes, such as keratin 6B (KRT6B), S100 calcium-binding protein A8 (S100A8), and crystallin alpha B (CRYAB). Meanwhile, genes associated with drug resistance (e.g., lysine demethylase 5B [KDM5B]) and radiation resistance (e.g., carnitine palmitoyltransferase 1A [CPT1A]) were also upregulated, confirming findings from other experimental analyses at the RNA level. In conclusion, this study successfully constructed a 3DP-based preclinical model for NPC research and proved its reliability and significant potential for advancing drug screening and mechanistic studies.

Keywords: 3D bioprinting; Drug screening; *In vitro* model; Nasopharyngeal carcinoma

†These authors contributed equally to this work.

***Corresponding authors:**
Huayu Yang
(dolphinyahy@hotmail.com)

Yilei Mao
(pumch-liver@hotmail.com)

Citation: Zhao H, Sun H, Yang H, Mao Y. Construction and application of a novel 3D bioprinting-based *in vitro* nasopharyngeal carcinoma model for drug screening and mechanistic research. *Int J Bioprint.* 2025;11(3):319-336. doi: 10.36922/IJB025040034

Received: January 26, 2025
1st revised: March 10, 2025
2nd revised: March 22, 2025
Accepted: March 28, 2025
Published online: March 28, 2025

1. Introduction

Nasopharyngeal carcinoma (NPC) is an epithelial carcinoma originating from the nasopharyngeal mucosa. According to the 2018 statistics, over 70% of new cases of NPC occur in East and Southeast Asia, with an age-standardized incidence rate of 3.0 cases per 100,000 people in China.[1] In recent years, the relationship between NPC and the Epstein-Barr Virus has become increasingly clear, providing a reliable clinical basis for early screening and diagnosis. It has been reported that the 5-year survival rate for early-stage patients after systemic treatment exceeds 70%.[2]

Radiotherapy is the primary treatment for NPC, supplemented by concurrent chemotherapy, induction chemotherapy, or adjuvant chemotherapy according to the Tumor Nodes Metastasis (TNM) stage of the tumor. Common chemotherapy drugs include cisplatin, docetaxel, paclitaxel, and 5-fluorouracil.[3] However, approximately 25% of patients with NPC still face poor prognoses due to local recurrence and distant metastasis,[2] which is mainly attributed to the drug resistance and radiation resistance of tumor cells. The specific mechanisms underlying this resistance remain unclear, largely due to the lack of reliable preclinical models for NPC research.

Traditional preclinical research models, which rely on cells cultured in two dimensions (2D-HK1), show significant limitations, primarily due to the lack of an environment similar to the *in vivo* extracellular matrix and three-dimensional (3D) cell–cell interactions.[4–8] In addition, tumor cells in the human body aggregate into cell masses. The gradient decline of oxygen and drug concentration from the periphery to the core of a tumor sphere results in differential effects of chemotherapy and radiotherapy on internal cells compared to those on the outer layer. Consequently, simple 2D cell cultures fail to accurately replicate the complex conditions of clinical treatment.[9,10] Therefore, there is an urgent need to establish an *in vitro* model that is similar to the tumor microenvironment *in vivo*. Such a model would better simulate the tumor's biological behavior, enhance understanding of radiobiological mechanisms, and improve preclinical drug screening.

These limitations have spurred on the development of new cell 3D culture technologies, such as spheroids, organoids, and 3D bioprinting (3DP), in recent years. Preclinical models of NPC have been successfully cultured using spheroid,[5,8–11] organoid,[2,7] and other technologies, with significant differences in protein expression, drug resistance, radiation resistance, and tumor cell invasiveness compared to traditional 2D models. However, each method has its challenges. Spheroids vary in size and are difficult to engineer consistently. Organoids, which must be generated from stem cells using a complex culture system, pose additional challenges, including high costs due to the need for Matrigel, size variability, poor reproducibility, and a lack of standardized evaluation methods.[12] Compared with other cell culture technologies, 3DP technology can construct 3D models with a shorter time and a higher cell activity. In addition, the printing process relies on precise computer programming, allowing it to construct more complex 3D geometric models with superior uniformity and fineness.[13,14] These attributes give this method natural advantages and huge engineering potential in the reconstruction of 3D *in vitro* models.[15–21]

In this study, we aimed to create a 3D human NPC model (3DP-HK1) *in vitro* using the NPC cell line HK1 with gelatin methacryloyl (GelMA) through extrusion-based 3DP technology (Figure 1). We observed significant differences between the 3D model and 2D cultured tumor cells, with the former demonstrating its advantages in simulating the tumor microenvironment *in vitro*. This study provides a new preclinical model for studying cell–extracellular matrix interactions, radiobiology, and chemotherapy drug screening in NPC.

2. Methods

2.1. Cell culture

Human NPC cell line HK1 was purchased from Guangzhou Yuanjing Biotechnology Co., LTD (China). The cells were cultured in Roswell Park Memorial Institute (RPMI) 1640 medium (Gibco, USA) containing 10% fetal bovine serum (Gibco, USA) and 1% penicillin-streptomycin (Gibco, USA). Routine cell culture was performed in an incubator maintained at 37°C with 5% CO_2, with media changes every 3 days and routine passage.

2.2. Construction of 3DP-HK1 model

The cells were expanded and cultured in a 2D system. Once reaching confluence, the cells were trypsinized and counted for preparing cell suspension. This suspension was mixed with 12.5% GelMA (EFL, China) at a ratio of 3:2 to create a bio-ink containing 5% GelMA with high-density HK1 cells at a concentration of 1×10^7 cells/mL. A photoinitiator, 2.5% lithium phenyl-2-4-6-trimethylbenzoylphosphinate (LAP; SUNP, China), was added at a certain volume ratio to achieve a final LAP concentration of 0.1%. The bio-ink was allowed to stand at 4°C for 10 min to enhance its printability. After gelation, the bio-ink was printed into 24-well plates in an $8 \times 8 \times 1.2$ mm^3 mesh structure under aseptic conditions using a high-precision extrusion 3D bioprinter (SUNP, SPP1603, China). The layer height was set to 0.2 mm, resulting in six layers. Printing parameters included a print speed of 8 mm/s and an extrusion speed of

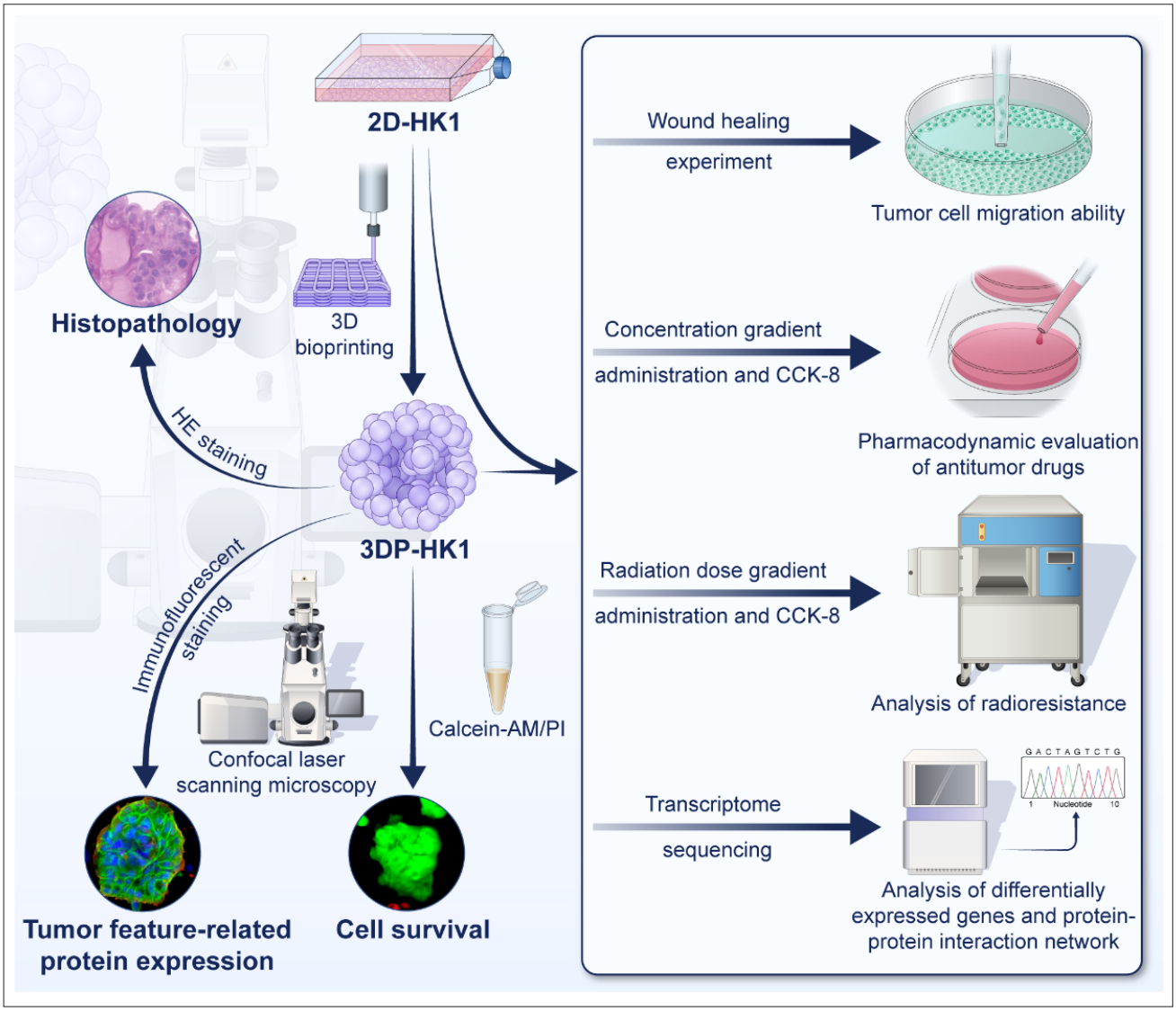

Figure 1. Schematic diagram depicting the route for employing 3DP-HK1 in research. Cell survival is analyzed after incubation with Calcein acetoxymethyl ester (Calcein-AM) and propidium iodide (PI) mixture. Histopathological features and tumor feature-related protein expression are observed, following hematoxylin and eosin (HE) staining and immunofluorescent staining, respectively. Wound healing experiment is conducted to test cell migration ability for both 3DP-HK1 and 2D-HK1. In terms of resistance to chemotherapy and radiotherapy, the differences between 3DP-HK1 and 2D-HK1 are analyzed by gradient administration of drug concentration and radiation dose. The advantage of 3DP-HK1 model is further verified at RNA level by means of transcriptome sequencing.

1.2 mm^3/s. The light curing intensity was set to 15%, with a curing period of 20 s. After printing, the models were cultured in the prepared medium, with routine medium changes every 3 days.

2.3. Cell survival in 3DP-HK1

Cell survival was observed and photographed on the 1st, 3rd, 6th, 9th, 12th, 15th, 18th, and 21st days after printing. The procedure is as follows: 3DP-HK1 was washed with phosphate-buffered saline (PBS; Servicebio, China), followed by the addition of Calcein-AM (Sigma, USA) and PI (Sigma, USA) mixture. The models were incubated in darkness for 25–30 min at 37 °C. After incubation, the models were washed with PBS again. A laser-scanning confocal microscope (Nikon, C2/C2si, Japan) was used to capture five random fields of view. ImageJ software (National Institutes of Health, USA) was used to count the cells in the photographed samples. Cell viability was calculated as follows: (live cells/total cells) × 100%.

2.4. Analysis of histopathological features of 3DP-HK1

The prints were stained with hematoxylin and eosin (HE) on the 12th day after printing, and the histopathological features were observed with a microscope. The cell mass diameter was measured using microscopic image processing software.

2.5. Detection and analysis of tumor feature-related protein expression

3DP-HK1 and 2D-HK1 models were fixed, permeabilized, and blocked at room temperature. Then, double staining was performed using the following primary antibody combinations: SRY-box transcription factor 2 (SOX2) mouse antibody (1:100, Proteintech, USA) with CD44 rabbit antibody (1:100, Proteintech, USA) and mouse antibody to integrin β1 (1:50, Abcam, USA) with integrin-linked kinase (ILK) rabbit antibody (1:200, Proteintech, USA). The samples were incubated with the primary antibodies overnight at 4 °C. Subsequently, the models were incubated for 2 h at room temperature with secondary antibodies: goat anti-rabbit antibodyIgG Alexa Fluor® 488 (1:200, Abcam, USA) and goat anti-mouse antibody IgG Alexa Fluor® 594 (1:200, Abcam, USA). Additionally, 4′,6-diamidino-2-phenylindole (DAPI) dye solution (1:500, Abcam, USA) was used to stain and localize the nuclei, with a 15-min incubation period at room temperature. The results of immunofluorescence staining were observed and photographed using a laser-scanning confocal microscope.

2.6. Cell migration ability test

On the 12th day after printing, the 3D models were lysed with GelMA lysis solution (EFL, China) and digested with trypsin (Gibco, USA) to create a single-cell suspension. The cells were then counted and seeded into six-well plates at an initial cell volume of 5×10^5 cells/well. The same procedure for digestion, counting, and seeding was applied to 2D-cultured cells. The cells were incubated overnight in RPMI 1640 medium containing 10% fetal bovine serum (cell density up to 100%). Single-layer cells were scratched in each hole using a 200 μL pipette tip. The old medium was discarded, and the wells were washed twice with PBS to remove the dislodged cells. Serum-free RPMI 1640 medium was then added. Scratch widths were observed under an optical microscope at 0, 3, 6, 9, 12, 24, 36, and 48 h. The wound closure ratio was calculated as = (Scratch widths at 0 h – Scratch widths at *n* h)/Scratch widths at 0 h × 100%. Differences between the 2D and 3D groups were analyzed and compared at each time point.

2.7. Pharmacodynamic evaluation of chemotherapy drugs

3DP-HK1 and 2D-HK1 were treated with cisplatin (MCE, USA) at concentrations of 0.1, 1, 5, 10, 20, 50 μM; paclitaxel (MCE, USA) at 0.0001, 0.001, 0.01, 0.1, 0.5, 1, 5, 10 μM; and 5-fluorouracil (Selleck, USA) at 0.01, 0.1, 1, 5, 10, 50, 100 μM on day 9 after printing. After 48 h of incubation, Cell Counting Kit-8 (CCK-8; Beyotime, China) was used to detect the effect of the chemotherapy drugs on tumor cell activity. The dose–response curve was plotted with GraphPad Prism 10 to calculate the half-inhibitory concentration (IC_{50}) for each drug. The results from the 3DP-HK1 and 2D-HK1 groups were then compared and analyzed.

2.8. Radioresistance analysis

3DP-HK1 and 2D-HK1 were subjected to irradiation at doses of 0, 2, 4, 6, 8, and 10 Gy on the 9th day after printing. After 6 days of continued culture, CCK-8 was used to measure optical density at 450 nm (OD450), reflecting the effect of radiation on tumor cell viability. Dose–response curves were fitted using GraphPad Prism 10, and the half-suppressed dose (ID_{50}) was calculated. The radioresistance of the 3DP-HK1 and 2D-HK1 groups was then compared and analyzed.

2.9. Transcriptomic sequencing and bioinformatics analysis

3DP-HK1 cells were lysed using GelMA lysis solution, and total RNA was extracted from both 3DP-HK1 and 2D-HK1 using TRIzol (Invitrogen, USA). RNA purity, integrity, and degradation were assessed. Sequencing libraries were generated using the NEBNext UltraTM RNA Library Prep Kit for Illumina, and sequencing was performed on the Illumina Hiseq 4000 platform. The DeSeq2 package was used to analyze differentially expressed genes (DEGs) ($p_{adj} < 0.05$), and the clusterProfiler R package was used for Gene Ontology (GO) and Kyoto Encyclopedia of Genes and Genomes (KEGG) enrichment analysis. Protein–protein interaction (PPI) networks were performed using the STRING database. Gene expression related to tumor malignancy, drug resistance, and radioresistance was examined to explore the mechanisms underlying tumorigenesis, chemotherapy resistance, and radiotherapy resistance in NPC.

2.10. Statistical analysis

The statistical results are expressed as mean ± standard deviation. Statistical analysis was performed using Student's *t*-test. *p*-value < 0.05 was considered statistically significant. Graphs were plotted using the GraphPad Prism version 10.0 software (GraphPad Software Inc., USA).

3. Results

3.1. Cell survival in 3DP-HK1

The cell mass, similar to an *in vivo* tumor, was photographed using a laser-scanning confocal microscope (Figure 2A). Calcein-AM and PI co-staining and ImageJ

analysis successfully verified that HK1 maintained good activity in 5% GelMA (the cell activities at day 1, 3, 6, 9, 12, 15, 18, and 21 after printing were 99.58 ± 0.12%, 95.03 ± 0.93%, 95.64 ± 0.79%, 96.13 ± 0.70%, 89.50 ± 2.02%, 93.11 ± 1.20%, 92.89 ± 1.36%, and 89.07 ± 1.92%, respectively) (Figure 2B).

3.2. Histopathological features of 3DP-HK1

After HE staining of 3DP-HK1, the malignant characteristics of tumor cells were clearly observed under an inverted optical microscope, including disordered arrangement, inconsistent cell size and shape, increased nucleo-cytoplasmic ratio, and significant differences in nuclear size and shape. Additionally, the cells formed

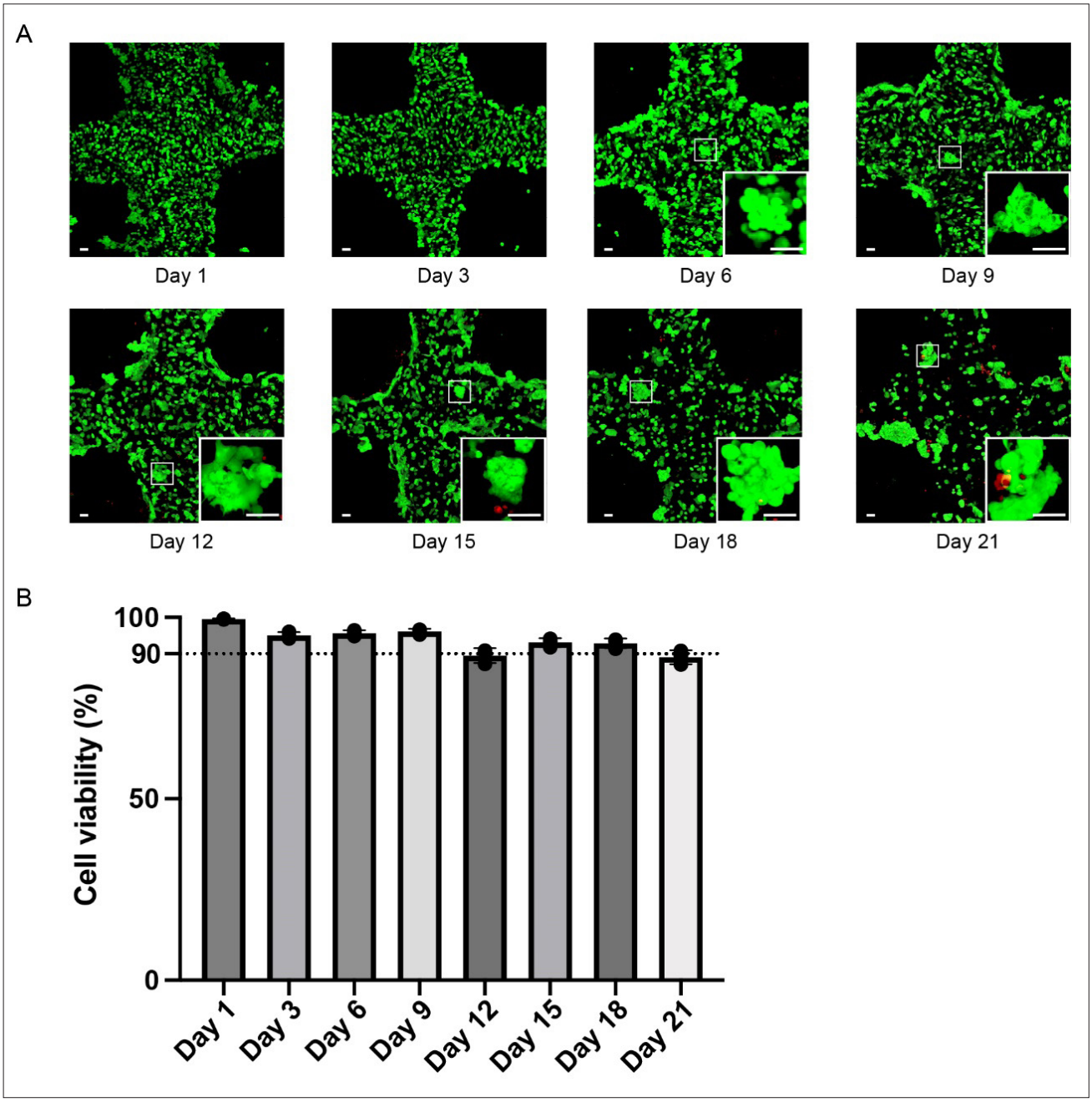

Figure 2. Cell activity at day 1, 3, 6, 9, 12, 15, 18, and 21 after printing. (A) Calcein-AM-stained surviving cells are shown in green, and PI-stained dead cells are shown in red. Scale bar: 50 μm. (B) Histograms of cell relative activity at day 1, 3, 6, 9, 12, 15, 18, and 21 after printing. All values are expressed as means ± SD.

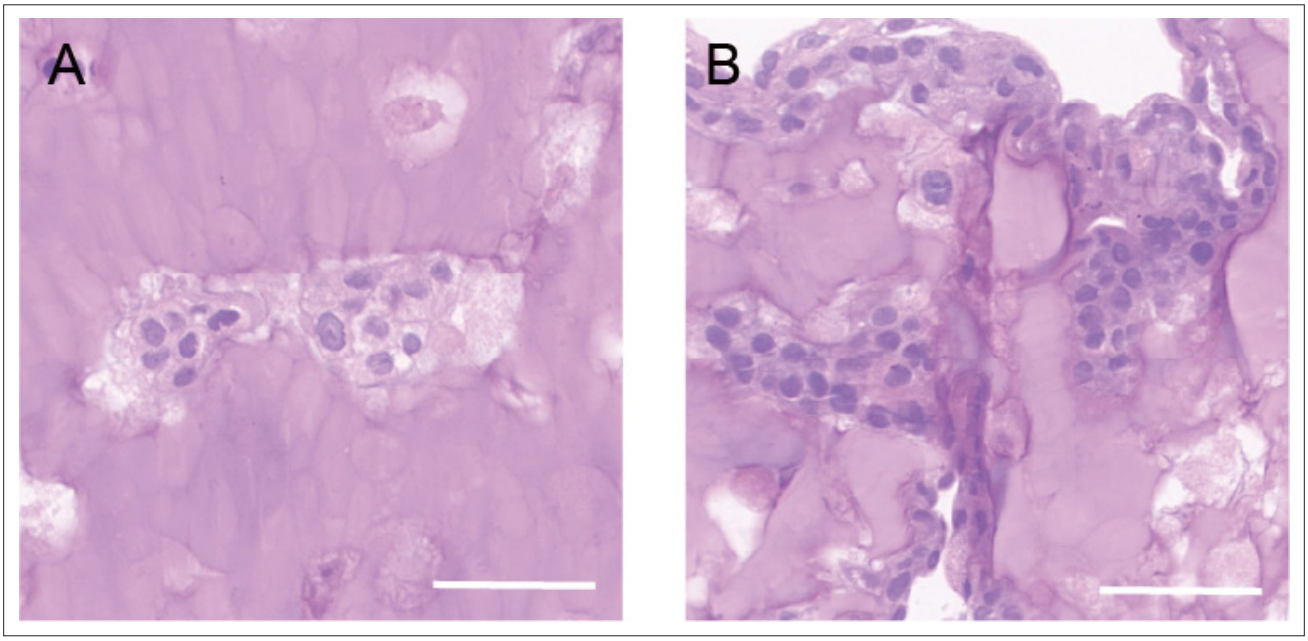

Figure 3. Hematoxylin and eosin staining of 3DP-HK1. Tumor cells with marked atypia appear in irregular nest. Keratinized substance can be seen at the center of the "cancer nest." Scale bar: 50 μm.

cell masses with the typical "cancer nest" characteristics of highly differentiated squamous cell carcinoma (Figure 3). Therefore, the experiment demonstrated that some histopathological features of the tumor can be reproduced *in vitro* by 3DP.

3.3. Detection of tumor feature-related protein expression

Detection of tumor feature-related protein expression is important to validate the advantages of the 3DP-HK1 model compared with the 2D-HK1 model. The expression of SOX2, CD44, integrin β1, and ILK in 3DP-HK1 and 2D-HK1 was observed using immunofluorescence staining and laser scanning confocal microscopy (Figure 4). The results showed that 3DP-HK1 effectively retained the expression of these specific proteins, proving that the 3DP-HK1 model has typical tumor characteristics and can serve as a model for evaluating future targeted therapies.

3.4. Evaluation of cell migration ability

To evaluate whether 3DP-HK1 showed better performance in invasion and metastasis than 2D-cultured cells, tumor cells in 3DP-HK1 were lysed and digested, then inoculated into six-well plates for the wound healing experiment on the 12th day after printing. 2D cultured cells were inoculated into six-well plates as controls. The wound closure ratios for 2D-HK1 at 3, 6, 9, 12, 24, 36, and 48 h were 5.09 ± 2.44%, 8.22 ± 2.59%, 11.41 ± 3.97%, 14.97 ± 0.92%, 26.34 ± 9.10%, 32.98 ± 8.72%, and 36.31 ± 3.23%, respectively. For 3DP-HK1, the wound closure ratios at 3, 6, 9, 12, and 24 h were 10.53 ± 2.39%, 14.33 ± 1.36%, 27.61 ± 5.94%, 32.73 ± 5.08%, and 57.26 ± 1.37%, respectively. At 36 h, only small, scattered scratches remained in 3DP-HK1, and by 48 h, the scratches were completely closed, achieving a closure rate of 100% (Figure 5A and B). These results showed that the migration ability of HK1 cells cultured in 3D model was significantly stronger than that of cells cultured in 2D model.

3.5. Analysis of drug resistance of 3DP-HK1 to chemotherapy

To test the resistance of 3DP-HK1 to first-line chemotherapy drugs for NPC, 3DP-HK1 and 2D-HK1 were treated with cisplatin, paclitaxel, and 5-fluorouracil on the 9th day after printing for 48 h, according to the concentration gradient. The OD450 values were measured using CCK-8. The relative cell viabilities of 3DP-HK1 cells treated with cisplatin at concentrations of 0.1, 1, 5, 10, 20, and 50 μM were 100.00 ± 5.30%, 100.66 ± 6.90%, 83.53 ± 4.02%, 80.07 ± 5.93%, 36.54 ± 2.15%, and 14.42 ± 0.41%, respectively. In contrast, the relative cell viabilities of 2D-HK1 cells under the same conditions were 100.00 ± 2.13%, 90.00 ± 2.63%, 34.29 ± 0.75%, 37.08 ± 1.08%, 26.41 ± 1.20%, and 12.16 ± 0.40%, respectively. When treated with paclitaxel at concentrations of 0.0001, 0.001, 0.01, 0.1, 0.5, 1, 5, and 10 μM, the relative cell viabilities of 3DP-HK1 cells were 100.00 ± 1.70%, 94.77 ± 0.86%, 80.96 ± 2.84%, 55.22 ± 0.73%, 51.64 ± 4.68%, 52.90 ± 3.90%,

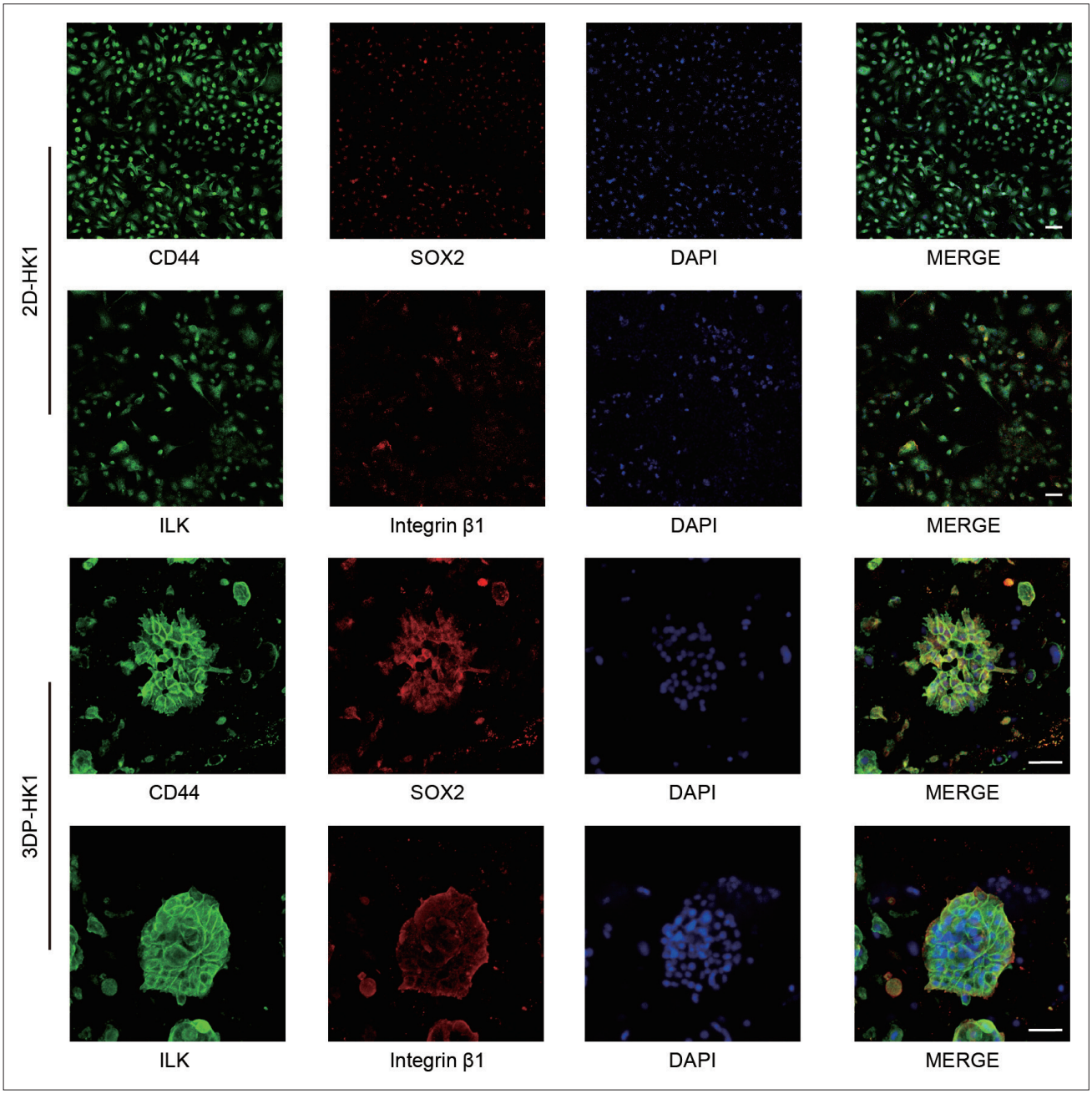

Figure 4. Immunofluorescence staining of tumor feature-related proteins in 3DP-HK1 and 2D-HK1. CD44, located on the cell membrane, is stained green, while SOX2, located in the nucleus, is stained red. ILK, also located on the cell membrane, is stained green, and integrin β1, located on the cell membrane, is stained red. The nuclei, stained with DAPI, are shown in blue. Scale bar: 50 μm.

13.25 ± 0.28%, and 11.52 ± 0.11%, respectively. For 2D-HK1 cells, the corresponding values were 100.00 ± 2.15%, 96.27 ± 2.52%, 56.34 ± 2.55%, 33.38 ± 1.02%, 28.62 ± 2.55%, 12.18 ± 1.87%, 6.62 ± 0.12%, and 5.45 ± 0.09%, respectively. Following treatment with 5-fluorouracil at concentrations of 0.01, 0.1, 1, 5, 10, 50, and 100 μM, the relative cell viabilities of 3DP-HK1 cells were 100.00 ± 4.01%, 94.56 ± 2.18%, 94.47 ± 2.12%, 88.75 ± 1.35%, 88.62 ± 1.49%, 66.21 ± 1.66%, and 59.34 ± 2.35%, respectively. In comparison, the relative cell viabilities of 2D-HK1 cells were 100.00 ± 3.42%, 97.62 ± 2.59%, 96.66 ± 3.10%, 90.46 ± 1.84%, 83.04 ± 2.22%, 49.56 ± 2.30%, and 43.61 ± 2.77%, respectively. Dose–response curves were generated using GraphPad Prism 10 to calculate IC_{50} values. The results showed that 3DP-HK1 showed significant chemotherapy resistance compared with 2D-HK1, demonstrating its

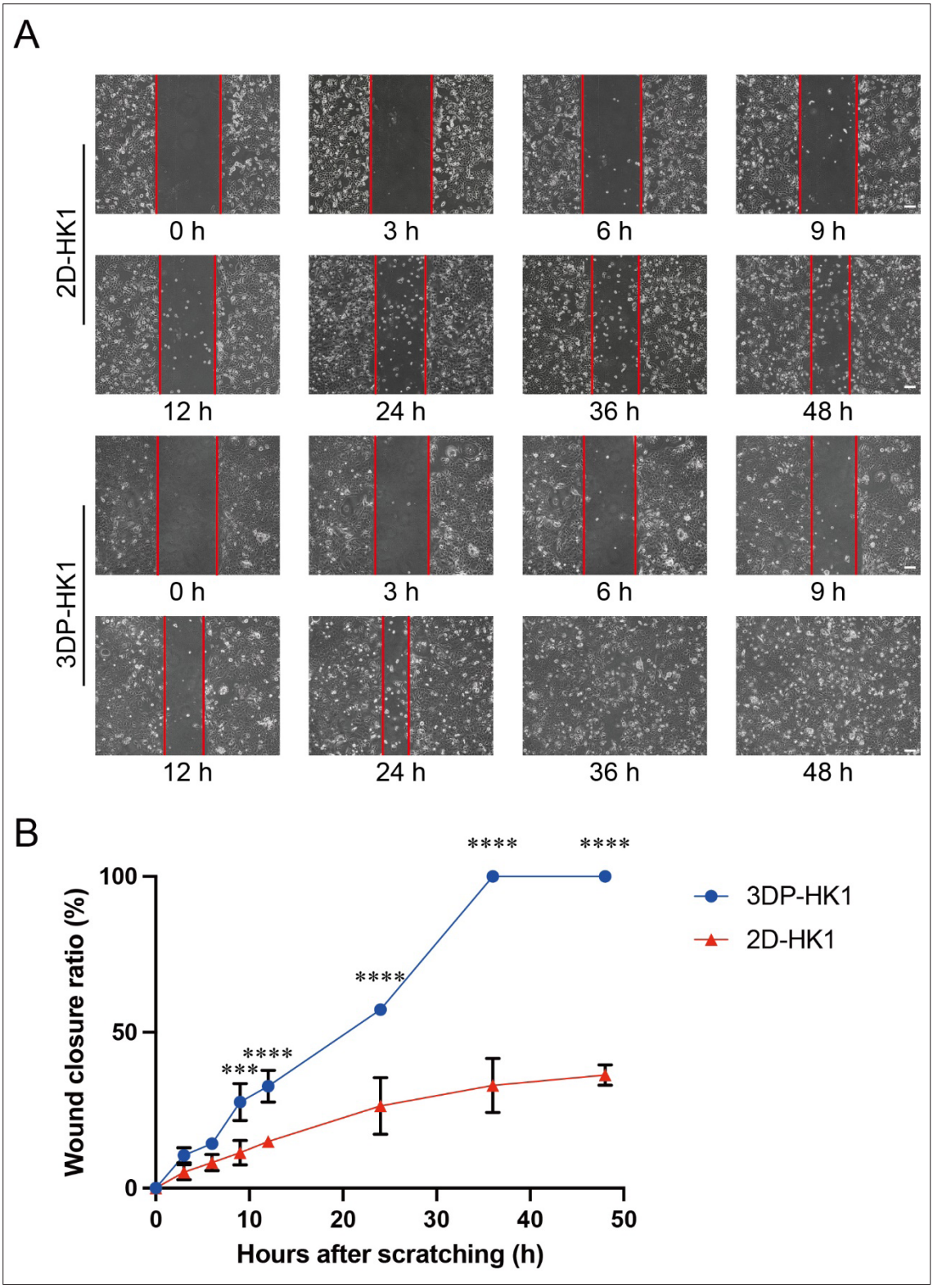

Figure 5. Results of the wound healing experiment. (A) Cell migration of 3DP-HK1 and 2D-HK1 at 0, 3, 6, 9, 12, 24, 36, 48 h after scratching. The red lines represent the boundaries between cells and scratches. Scale bar: 100 μm. (B) Wound closure ratios of 3DP-HK1 and 2D-HK1 at each time point. All values are expressed as means ± SD. ***$p < 0.001$; ****$p < 0.0001$.

potential as a reliable model for studying drug resistance mechanisms. The IC_{50} values for cisplatin in 3DP-HK1 and 2D-HK1 were 16.73 and 4.69 μM, respectively (Figure 6A). The IC_{50} values for paclitaxel in 3DP-HK1 and 2D-HK1 were 0.360 and 0.036 μM, respectively (Figure 6B). The IC_{50} values for 5-fluorouracil in 3DP-HK1 and 2D-HK1 were 177.10 and 61.55 μM, respectively (Figure 6C).

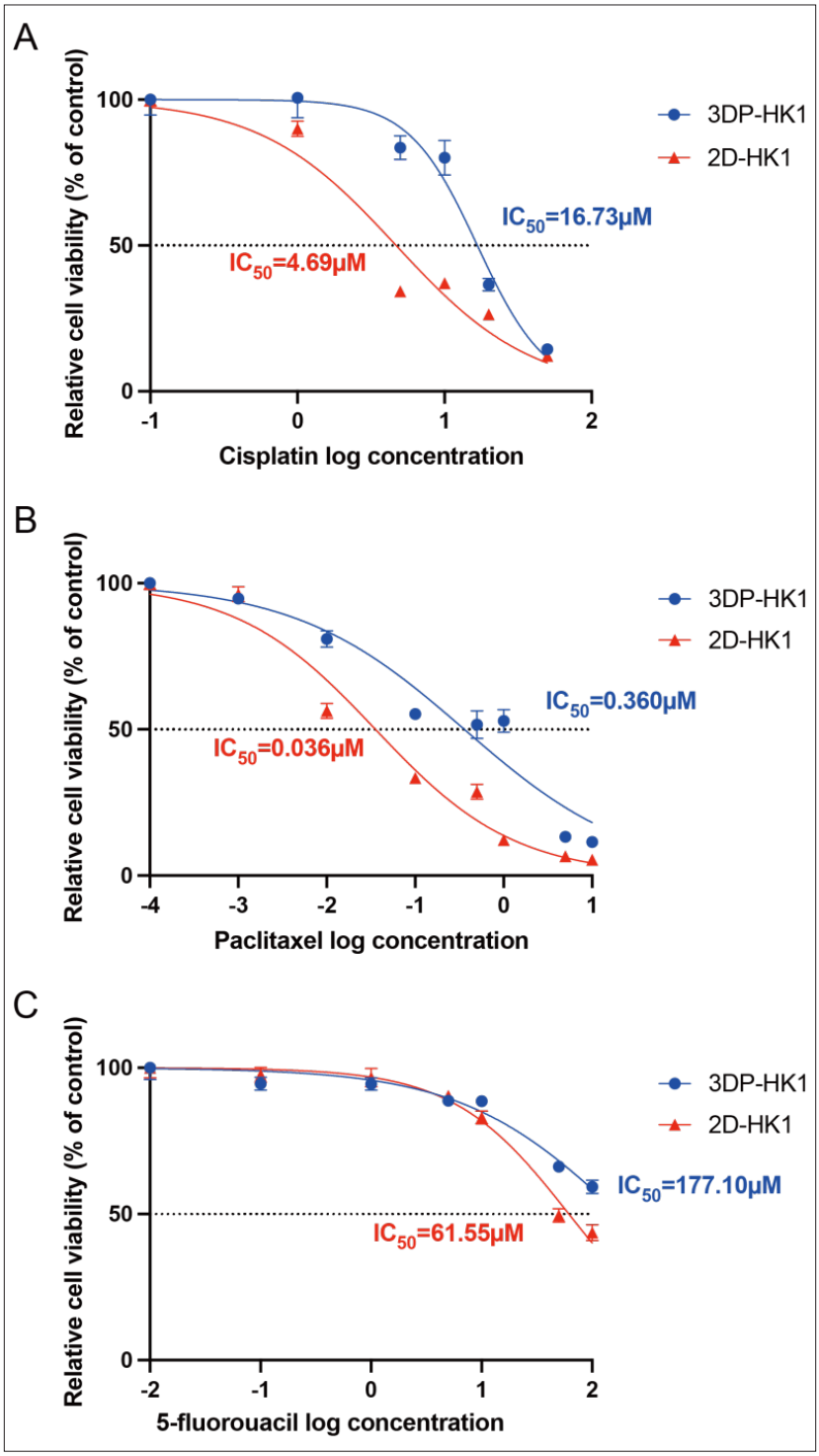

Figure 6. Dose–response curves of cisplatin (A), paclitaxel (B), and 5-fluorouracil (C) in 3DP-HK1 and 2D-HK1 48 h after administration. All values are expressed as means ± SD.

3.6. Analysis of cell activity after radiotherapy

Radiotherapy is a conventional treatment for NPC, but some patients have low sensitivity to radiotherapy, so they are ending up with poor-treatment outcomes. To evaluate the difference in radiotherapy sensitivity between 3DP-HK1 and 2D-HK1, both models were irradiated according to the radiation dose gradient (0, 2, 4, 6, 8, 10 Gy) on the 9th day after printing. They were then cultured for an additional 6 days with routine media changes. Cell viability in both 3DP-HK1 and 2D-HK1 after radiotherapy was measured using CCK-8. The relative cell viabilities of 3DP-HK1 irradiated to 0, 2, 4, 6, 8, and 10 Gy were 100.00 ± 0.24%, 94.61 ± 0.90%, 85.12 ± 1.18%, 79.13 ± 1.78%, 76.60 ± 3.62%, and 75.33 ± 1.41%, respectively; while those of 2D-HK1 were 100.00 ± 0.74%, 111.42 ± 1.25%, 91.22 ± 1.07%, 67.81 ± 1.03%, 47.47 ± 1.63%, and 31.66 ± 0.62%, respectively. Dose–response curves were generated, and the ID_{50} values were calculated using GraphPad Prism 10. The results showed that the ID_{50} values for 3DP-HK1 and 2D-HK1 were 32.43 and 7.77 Gy, respectively (Figure 7), indicating that 3DP-HK1 had higher radiotherapy resistance than 2D-HK1.

3.7. Transcriptomic feature analysis

The characteristic differences between 3DP-HK1 and 2D-HK1 at the transcriptome level were compared using total mRNA sequencing to verify whether a biomimetic tumor microenvironment was successfully constructed in 3DP-HK1. A total of 10,421 DEGs were identified, including 5471 upregulated DEGs and 4950 downregulated DEGs (Figure 8A and B). Notably, the expressions of genes, such as keratin 6B (*KRT6B*), annexin A1 (*ANXA1*), interferon-induced transmembrane protein 1 (*IFITM1*), and C-X-C motif chemokine ligand 10 (*CXCL10*), were significantly increased, while the expression of genes, including carbonyl reductase 3 (*CBR3*), were downregulated. These changes may be closely related to the occurrence and development of NPC. Furthermore, the expression of drug resistance genes, such as lysine demethylase 5B (*KDM5B*), and radiotherapy resistance genes, such as carnitine palmitoyltransferase 1A (*CPT1A*), was significantly upregulated in 3DP-HK1, which was consistent with the results from the drug sensitivity and radiotherapy sensitivity experiments (Figure 8C). In addition, GO enrichment analysis showed that upregulated DEGs were mainly enriched in pathways related to the "G1/S transition of the mitotic cell cycle," "autophagosome assembly," "transition metal ion transport," "very long-chain fatty acid metabolic process," "histone acetyltransferase complex," and "histone deacetylase complex" (Figure 9A). Conversely, downregulated DEGs were mainly enriched in pathways associated with "cell cycle checkpoint signaling," "mitotic sister chromatid segregation," "G1/S transition of the mitotic cell cycle," "DNA damage checkpoint signaling," "G2/M transition of the mitotic cell cycle," "regulation of DNA recombination,"

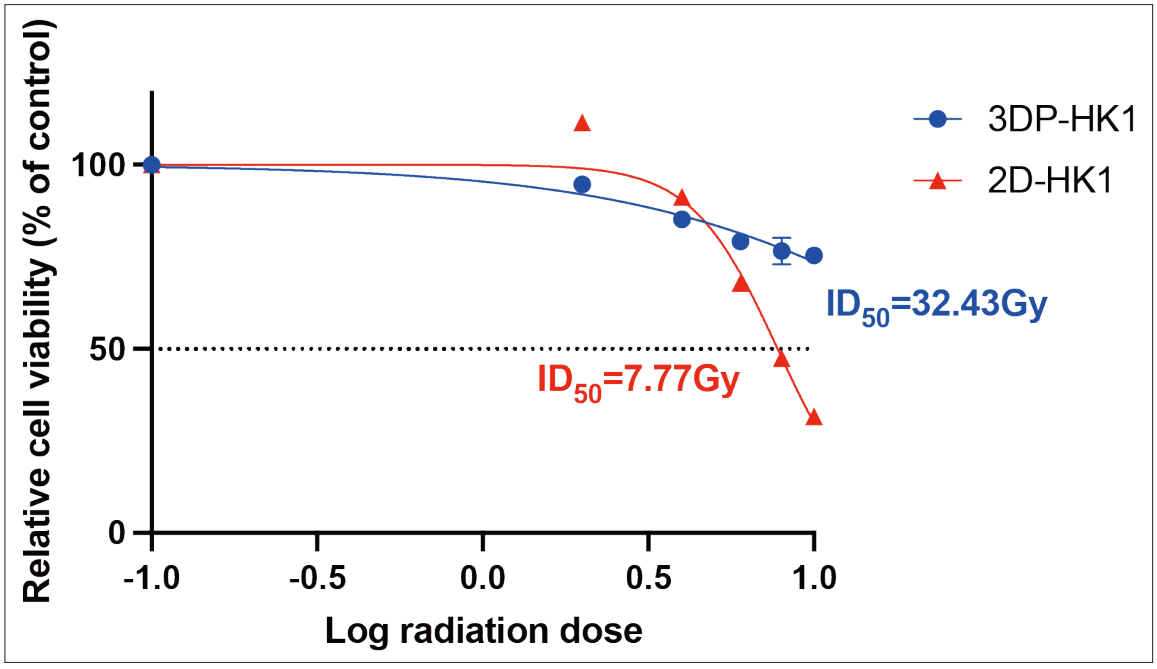

Figure 7. Dose–response curves of radiation exposure to 3DP-HK1 and 2D-HK1. There is a sharp decline for cell viability in 2D-HK1 with the increase of the radiation dose, while the curve for 3DP-HK1 is relatively smooth and stable. All values are expressed as means ± SD.

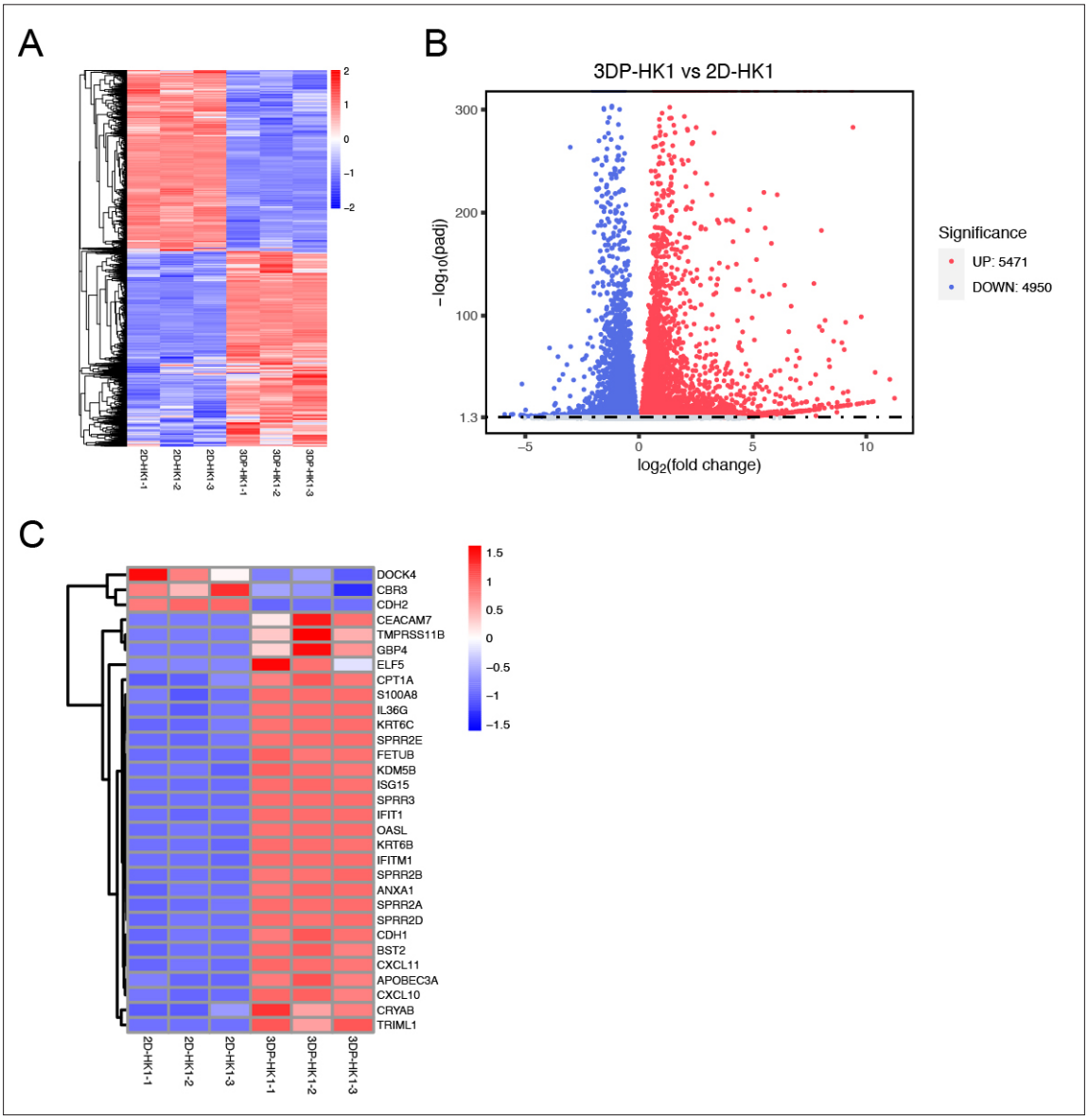

Figure 8. DEGs analysis of 3DP-HK1 and 2D-HK1. (A) Heatmap of all DEGs between the 3DP-HK1 and 2D-HK1 models. Rows represent genes, and columns represent samples. (B) Volcano plot showing 10,421 DEGs, including 5471 upregulated DEGs (red spots) and 4950 downregulated DEGs (blue spots). (C) Heatmap of some differentially expressed tumor-related genes between the 3DP-HK1 and 2D-HK1 models. Abbreviation: DEG, differentially expressed gene.

"regulation of cyclin-dependent protein serine/threonine kinase activity," "mitochondrial genome maintenance," "sulfur amino acid metabolic process," "ribosomal small subunit assembly," "DNA replication checkpoint signaling," "ribosomal subunit export from the nucleus," "ribosomal large subunit assembly," "mitotic spindle elongation," "sulfur amino acid biosynthetic process," "histone deacetylase complex," "nucleotide-excision repair complex," and "tRNA binding" (Figure 9B). KEGG enrichment analysis showed that upregulated DEGs were mainly enriched in pathways related to "Shigellosis," "Autophagy-animal," "TNF signaling pathway," "C-type lectin receptor signaling pathway," "Yersinia infection," and "Proteoglycans in cancer" (Figure 9C). In contrast, downregulated DEGs were mainly enriched in pathways related to the "Ribosome," "Cell cycle," "Spliceosome," "Amyotrophic lateral sclerosis," "Ribosome biogenesis in eukaryotes," and "Huntington's disease" (Figure 9D). The hub genes of the upregulated DEGs (e.g., E1A binding protein p300 [*EP300*] and CREB binding protein [*CREBBP*]) were

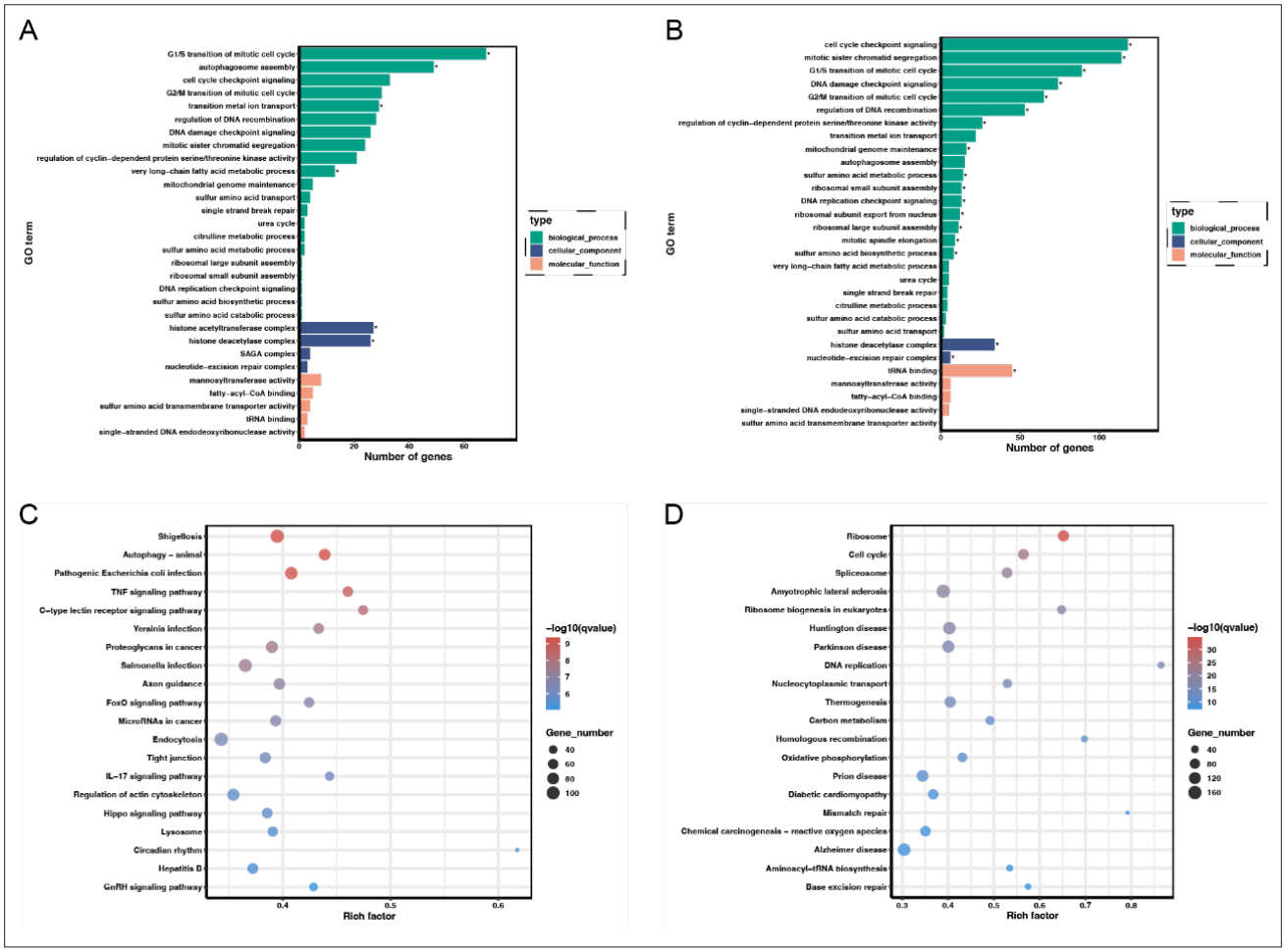

Figure 9. Functional enrichment analysis of 3DP-HK1. The most enriched GO terms for (A) upregulated DEGs and (B) downregulated DEGs in 3DP-HK1 versus 2D-HK1. The *x*-axis represents the number of genes, and the *y*-axis represents GO-enriched terms. Biological processes, cellular components, and molecular functions are distinguished by different colors. KEGG pathway enrichment bubble chart for (C) upregulated genes and (D) downregulated genes. The *x*-axis represents the rich factor, and the *y*-axis represents KEGG-enriched terms. The size of the dot represents the number of genes under a specific term, while the color of the dots represents the *q*-value. Abbreviations: GO, Gene Ontology; KEGG, Kyoto Encyclopedia of Genes and Genomes.

associated with embryonic development, growth control, cell proliferation, and differentiation (Figure 10A), while the hub genes of downregulated DEGs (e.g., cell division cycle 20 [*CDC20*] and exonuclease 1 [*EXO1*]), were mainly involved in regulating the cell cycle, mismatching repair, and recombination (Figure 10B).

Therefore, through the comparison and analysis of 3DP-HK1 and 2D-HK1 at the transcriptome level, it is evident that the two models have different tumor microenvironments and biological characteristics, which further proves the success of the 3DP-HK1 model.

4. Discussion

The mechanisms underlying NPC occurrence and development remain unclear, partly due to the limitations of the current research models of NPC. The most commonly used preclinical model is the immortalized NPC cell line.[7] However, cells cultured in two dimensions fail to accurately replicate the *in vivo* environment, particularly in terms of cell–cell and cell–extracellular matrix interactions in 3D conditions. Consequently, the research results, including those from chemotherapy drug screening, are not effectively translated into clinical application.[6,8–10] In addition, many established NPC cell lines have been found to be contaminated with HeLa cells, and their reliability for scientific research has been challenged.[22,23]

3DP, an increasingly advanced modeling technology, has been successfully applied in many fields[24–29] but has not yet been used for NPC modeling. In this study, we used GelMA to successfully develop a novel 3D *in vitro* model of NPC, which provides an environment that simulates the extracellular matrix for tumor cells.

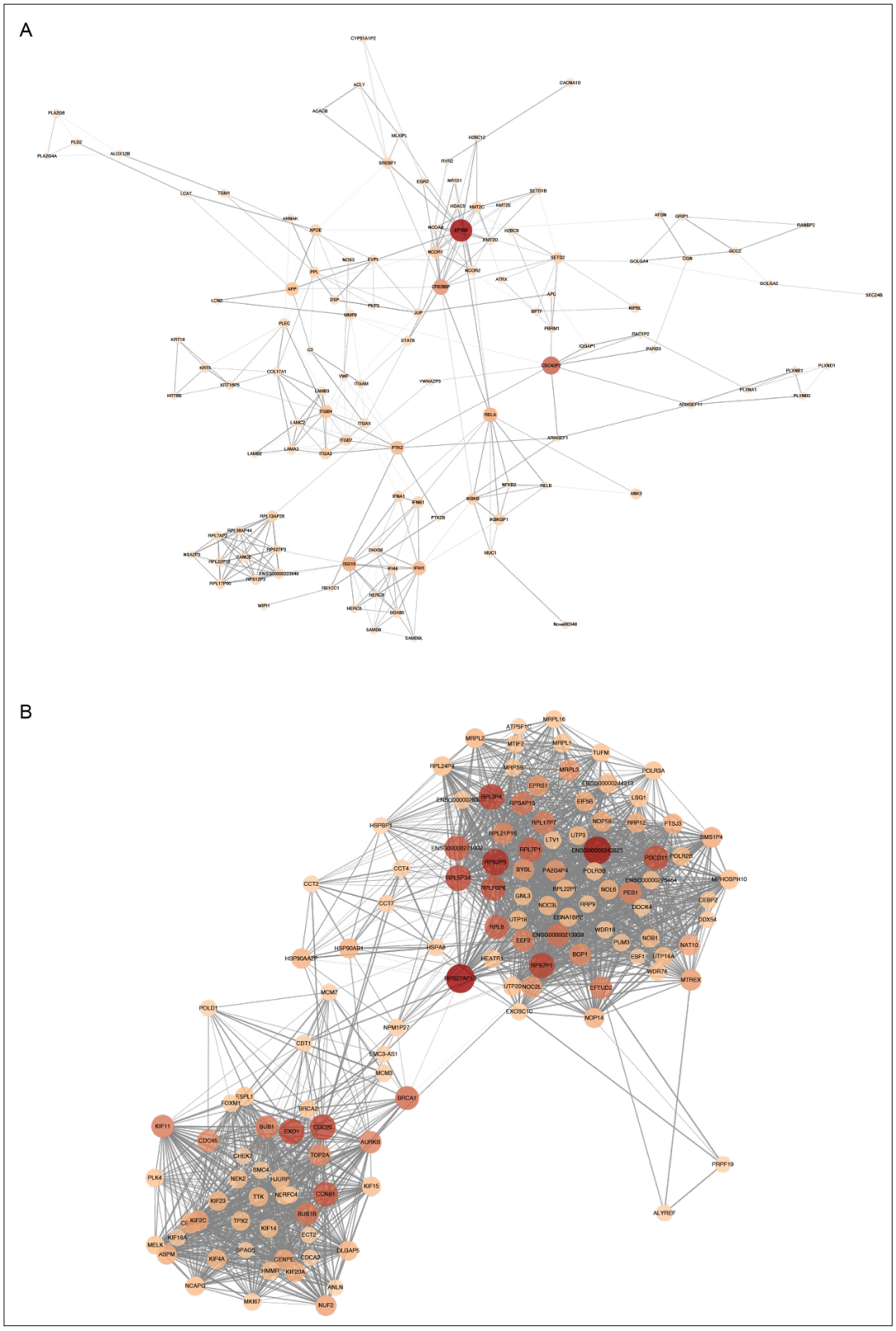

Figure 10. Protein–protein interaction networks of 3DP-HK1. The networks showed correlations between (A) upregulated genes (degree ≥ 5) and (B) downregulated genes (degree ≥ 30), where the thickness of the edge indicates the strength of the interaction, and the color and the size of the nodes indicate the degree of the corresponding gene.

This model evenly distributes tumor cells, which are not contaminated by HeLa cells, into geometries of specific sizes according to a preset density. We found that the tumor cells maintained high activity in the model, with significant changes in cell behavior and functional expression, similar to that of tumors *in vivo*. Specifically, the tumor cells formed cancer nest-like structures in the 3DP-based model, retained tumor-related protein expression, and exhibited significantly enhanced migration. In addition, the resistance of tumor cells to first-line chemotherapy drugs and radiotherapy for NPC increased significantly. Transcriptome sequencing indicated that 3DP-HK1 has a characteristic gene expression profile. Our results demonstrate that 3DP-based *in vitro* preclinical models of NPC have great potential for advancing related research.

The 3D model of NPC developed in this study is mainly based on extrusion 3DP technology. The entire printing process is precisely controlled by a preset program, ensuring the constructed model has high homogeneity. The operation is simple and easy to implement. The printing time is short, and the printing cost is low.[28,30] In addition, the cells can be fully extended in a 3D environment with sufficient space, overcoming the limitations of 2D culture and allowing for long-term culture. GelMA closely mimics the natural extracellular matrix by providing cell attachment sites and matrix metalloproteinase response peptide motifs, which allow cells to proliferate and spread in the GelMA-based scaffold.[31] When GelMA is exposed to light, it cross-links to form hydrogels with controllable mechanical properties. Many studies have shown that GelMA, among the new, emerging bio-inks for 3DP, has great potential in a wide range of applications.[32–35] Therefore, we decided to use 5% (w/v) GelMA + 0.1% (w/v) LAP as the bio-ink for this research.

For morphology and histopathological analysis, HE staining was performed on the model. The results revealed significant atypia in the tumor cells, including variations in size and shape, as well as a high nucleus-to-plasma ratio. As a highly differentiated squamous cell carcinoma, HK1 cells clustered into nests in the printed model, which had obvious advantages over the single spatial arrangement seen in 2D cultures.

SOX2 and CD44 have been reported as stemness markers in NPC, and their expression in NPC cells reflects proliferative and recurrent characteristics of 3DP-HK1.[36–38] In addition, integrins are known to play a critical role in tumor cell invasion and metastasis. Several studies have reported that integrin β1 and other cell adhesion molecules mediate the metastasis and progression of NPC.[39–41] By using immunofluorescence methods, we successfully confirmed the expression of SOX2, CD44, integrin β1, and integrin-linked kinase in 3DP-HK1 was well preserved. Therefore, 3DP-HK1 has typical NPC tumor characteristics at the protein level and is a valuable model for future targeted therapy studies.

To investigate the cell invasion and migration ability of 3DP-HK1 at the level of cell biological phenotype, we performed a classical wound healing experiment. The higher scratch closure rate of 3DP-HK1 indicated that its cell migration ability was better than that of 2D-cultured cells, which can be further explored to investigate the molecular mechanism underlying invasion and metastasis in NPC.

By using first-line chemotherapy drugs for NPC to test the drug sensitivity of the 3DP-HK1 model, we found that the IC_{50} values for cisplatin, paclitaxel, and 5-fluorouracil were significantly higher in the 3DP-HK1 model compared to 2D-HK1 model, which were closer to the effective blood concentration of these chemotherapy drugs in humans.[42–44] Therefore, before the drug development enters the clinical trial stage, it can be used to conduct pharmacodynamic and toxicity tests on 3DP-based models, providing more reliable results than traditional 2D-cultured cells. Thus, it can greatly reduce the failure rate of clinical trials and the time and cost of drug screening. Similarly, we exposed the cells to radiation to mimic clinical radiotherapy, and we found that 3DP-HK1 had higher ID_{50} results and a better correlation with the recommended dose of clinical radiotherapy.[3,45] Therefore, this model can be used to explore the reaction and tolerance mechanism of NPC tumor cells to radiation, helping to adjust and optimize clinical radiotherapy regimens for NPC.

To verify the reliability and superiority of the 3DP-HK1 model at the RNA level, we conducted total RNA sequencing. Compared with the transcriptomic data from 2D-HK1, 3DP-HK1 had unique transcriptional profile characteristics, which we attributed to the 3D culture environment. In the transcriptional profile of 3DP-HK1, we detected high expression levels of epithelial characteristic genes, including *KRT6B*, S100 calcium binding protein A8 (*S100A8*), crystallin alpha B (*CRYAB*), keratin 6C (*KRT6C*), CEA cell adhesion molecule 7 (*CEACAM7*), interleukin 36 gamma (*IL36G*), small proline rich protein 2E (*SPRR2E*), small proline rich protein 2A (*SPRR2A*), small proline rich protein 2D (*SPRR2D*), small proline rich protein 2B (*SPRR2B*), apolipoprotein B mRNA editing enzyme catalytic subunit 3A (*APOBEC3A*), fetuin B (*FETUB*), E74 like ETS transcription factor 5 (*ELF5*), tripartite motif family like 1 (*TRIML1*), transmembrane serine protease 11B (*TMPRSS11B*), and small proline rich protein 3

(*SPRR3*). According to Chen et al.,[46] this gene expression profile is characteristic of the NPC cells. Furthermore, according to a distant metastasis gene signature for locoregionally advanced NPC established by Tang et al.,[47] the upregulation of *ANXA1* and downregulation of *CBR3* in 3DP-HK1 may indicate enhanced metastasis ability of the tumor cells. Jin et al.[40] suggested that NPC cells have an epithelial-immune dual feature, with their immune characteristics positively correlated with the degree of malignancy. We also observed significant upregulation of immune-related genes, such as *IFITM1*, bone marrow stromal cell antigen 2 (*BST2*), guanylate binding protein 4 (*GBP4*), and 2′-5′-oligoadenylate synthetase like (*OASL*), in the transcription profile. In addition, NPC cells highly expressed T cell chemokines, including CXCL10 and C-X-C motif chemokine ligand 11 (CXCL11), consistent with the transcriptomic sequencing results of our 3DP-HK1 model. Weichselbaum et al.[48] reported that the upregulation of interferon-stimulated gene 15 (*ISG15*), interferon induced protein with tetratricopeptide repeats 1 (*IFIT1*), and other genes mediates drug and radiation resistance in tumor cells, a finding concurring with our transcription profile for the 3DP-HK1. Furthermore, upregulation of CPT1A[49] and downregulation of dedicator of cytokinesis 4 (DOCK4)[50] in 3DP-HK1 have been reported to mediate radiation resistance in NPC, while overexpression of KDM5B is associated with cisplatin resistance in NPC.[51] In addition, functional enrichment analysis and PPI networks also suggested the enrichment of tumor feature-related pathways in 3DP-HK1, such as cell cycle regulation and tumor necrosis factor (TNF) signaling. Notably, the expression of cadherin 1 (CDH1), which encodes E-cadherin, was upregulated, and cadherin 2 (CDH2), which encodes N-cadherin, was downregulated. These findings align with those of Fang et al.[9] in another 3D NPC model. According to the epithelial–mesenchymal transition theory, such changes do not correspond to the cell phenotype observed in our wound healing experiments, suggesting that NPC metastasis may not be driven by epithelial–mesenchymal transition mechanisms. Another interesting result was that upregulated DEGs were enriched in shigellosis and Yersinia infection in KEGG enrichment analysis. Based on the growing research findings on the tumor microbiome, this result may also suggest a delicate relationship between NPC and microorganism. In summary, the specificity of 3DP-HK1 at the transcriptome level demonstrates the advantages of this model over the 2D model in studying characteristic gene expression in NPC, offering insights into potential marker genes and mechanisms of chemotherapy and radiotherapy resistance.

5. Conclusion

In conclusion, we successfully constructed an *in vitro* NPC model by using 3DP and demonstrated its great potential for drug screening and mechanistic research on NPC. However, our study is not without limitations, warranting future research in certain areas. First, the 3DP-HK1 model we constructed lacks other key components of the tumor microenvironment, such as immune cells and stromal cells, which we predict also have a significant impact on tumor cell behavior. In addition, since surgical treatment is not the main treatment method for NPC, obtaining NPC specimens is challenging. Consequently, we did not use patient-derived primary cells for this study. Moving forward, we aim to expand on immortalized cell line models by constructing patient-derived 3DP-based NPC models using biopsied specimens. This approach will help advance personalized treatment strategies for patients with NPC.

Acknowledgments

None.

Funding

This work was supported by the CAMS Innovation Fund for Medical Sciences (2021-I2M-1-058), National High Level Hospital Clinical Research Funding (2022-PUMCH-B-034), and National Natural Science Foundation of China (32271470).

Conflict of interest

The authors declare no competing interests.

Authors' contributions

Conceptualization: Hang Sun
Funding acquisition: Huayu Yang, Yilei Mao
Investigation: Hang Sun, Haijie Zhao
Methodology: Hang Sun, Haijie Zhao
Project administration: Haijie Zhao, Hang Sun
Supervision: Huayu Yang, Yilei Mao
Visualization: Haijie Zhao
Writing–original draft: Haijie Zhao
Writing–review & editing: Hang Sun, Huayu Yang, Yilei Mao

Ethics approval and consent to participate

Not applicable.

Consent for publication

Not applicable

Availability of data and materials

Additional data and materials not included in the manuscript or supplementary materials are available from the corresponding authors upon reasonable request.

References

1. Chen YP, Chan ATC, Le QT, Blanchard P, Sun Y, Ma J. Nasopharyngeal carcinoma. *Lancet (London, England)*. 2019;394(10192):64-80. doi: 10.1016/S0140-6736(19)30956-0
2. Zhu H, Qu S, Deng Y, et al. Application of organoids in otolaryngology: head and neck surgery. *Eur Arch Otorhinolaryngol*. 2024;281(4):1643-1649. doi: 10.1007/s00405-023-08348-4
3. Tang L, Chen Y, Chen C, et al. The Chinese society of clinical oncology (CSCO) clinical guidelines for the diagnosis and treatment of nasopharyngeal carcinoma. *Cancer Commun*. 2021;41(11):1195-1227. doi: 10.1002/cac2.12218
4. Hong X, Xu Y, Pang SW. Enhanced motility and interaction of nasopharyngeal carcinoma with epithelial cells in confined microwells. *Lab Chip*. 2023;23(3):511-524. doi: 10.1039/d2lc00616b
5. Muniandy K, Sankar PS, Xiang BLS, Soo-Beng AK, Balakrishnan V, Mohana-Kumaran N. Establishment and analysis of the 3-dimensional (3D) spheroids generated from the nasopharyngeal carcinoma cell line HK1. *Trop Life Sci Res*. 2016;27(suppl 1):125-130. doi: 10.21315/tlsr2016.27.3.17
6. Yi C, Lai SL, Tsang CM, et al. A three-dimensional spheroid-specific role for wnt-β-catenin and eph-ephrin signaling in nasopharyngeal carcinoma cells. *J Cell Sci*. 2021;134(16):jcs256461. doi: 10.1242/jcs.256461
7. Wang XW, Xia TL, Tang HC, et al. Establishment of a patient-derived organoid model and living biobank for nasopharyngeal carcinoma. *Ann Transl Med*. 2022; 10(9):526. doi: 10.21037/atm-22-1076
8. Teh JL, Abdul Rahman SF, Domnic G, et al. Rapid spheroid assays in a 3-dimensional cell culture chip. *BMC Res Notes*. 2021;14(1):310. doi: 10.1186/s13104-021-05727-0
9. Fang Y, Liang S, Gao J, et al. Extracellular matrix stiffness mediates radiosensitivity in a 3D nasopharyngeal carcinoma model. *Cancer Cell Int*. 2022;22(1):364. doi: 10.1186/s12935-022-02787-5
10. Ngaokrajang U, Janvilisri T, Sae-Ueng U, Prungsak A, Kiatwuthinon P. Integrin α5 mediates intrinsic cisplatin resistance in three-dimensional nasopharyngeal carcinoma spheroids via the inhibition of phosphorylated ERK /caspase-3 induced apoptosis. *Exp Cell Res*. 2021;406(2):112765. doi: 10.1016/j.yexcr.2021.112765
11. Wu RWK, Chu ESM, Yuen JWM, Huang Z. Comparative study of FosPeg® photodynamic effect on nasopharyngeal carcinoma cells in 2D and 3D models. *J Photochem Photobiol B*. 2020;210:111987. doi: 10.1016/j.jphotobiol.2020.111987
12. Huch M, Knoblich JA, Lutolf MP, Martinez-Arias A. The hope and the hype of organoid research. *Development (Cambridge, England)*. 2017;144(6):938-941. doi: 10.1242/dev.150201
13. Kim J, Kim J, Gao G, et al. Bioprinted organoids platform with tumor vasculature for implementing precision personalized medicine targeted towards gastric cancer. *Adv Funct Mater*. 2024;34(11):2306676. doi: 10.1002/adfm.202306676
14. Chen H, Cheng Y, Wang X, et al. 3D printed in vitro tumor tissue model of colorectal cancer. *Theranostics*. 2020;10(26):12127-12143. doi: 10.7150/thno.52450
15. Burkholder-Wenger AC, Golzar H, Wu Y, Tang XS. Development of a hybrid Nanoink for 3D bioprinting of heterogeneous tumor models. *ACS Biomater Sci Eng*. 2022;8(2):777-785. doi: 10.1021/acsbiomaterials.1c01265
16. Li S, Liu S, Wang X. Advances of 3D printing in vascularized organ construction. *Int J Bioprint*. 2022;8(3):588. doi: 10.18063/ijb.v8i3.588
17. Ma X, Liu J, Zhu W, et al. 3D bioprinting of functional tissue models for personalized drug screening and in vitro disease modeling. *Adv Drug Delivery Rev*. 2018;132:235-251. doi: 10.1016/j.addr.2018.06.011
18. Ma X, Yu C, Wang P, et al. Rapid 3D bioprinting of decellularized extracellular matrix with regionally varied mechanical properties and biomimetic microarchitecture. *Biomaterials*. 2018;185:310-321. doi: 10.1016/j.biomaterials.2018.09.026
19. Matai I, Kaur G, Seyedsalehi A, McClinton A, Laurencin CT. Progress in 3D bioprinting technology for tissue/ organ regenerative engineering. *Biomaterials*. 2020; 226:119536. doi: 10.1016/j.biomaterials.2019.119536
20. Sbirkov Y, Molander D, Milet C, et al. A colorectal cancer 3D bioprinting workflow as a platform for disease modeling and chemotherapeutic screening. *Front Bioeng Biotechnol*. 2021;9:755563. doi: 10.3389/fbioe.2021.755563
21. Xu J, Yang S, Su Y, et al. A 3D bioprinted tumor model fabricated with gelatin/sodium alginate/decellularized extracellular matrix bioink. *Int J Bioprint*. 2023;9(1):630. doi: 10.18063/ijb.v9i1.630

22. Strong MJ, Baddoo M, Nanbo A, Xu M, Puetter A, Lin Z. Comprehensive high-throughput RNA sequencing analysis reveals contamination of multiple nasopharyngeal carcinoma cell lines with HeLa cell genomes. *J Virol*. 2014;88(18):10696-10704.
doi: 10.1128/JVI.01457-14

23. Makowska A, Kontny U, Weiskirchen R. HeLa cells cross-contaminated nasopharyngeal carcinoma cell lines: Still a common problem. *Br J Cancer*. 2024;130(12):1885-1886.
doi: 10.1038/s41416-024-02675-x

24. Fan Z, Wei X, Chen K, Wang L, Xu M. 3D bioprinting of an endothelialized liver lobule-like construct as a tumor-scale drug screening platform. *Micromachines*. 2023;14(4):878.
doi: 10.3390/mi14040878

25. Li Y, Zhang T, Pang Y, Li L, Chen ZN, Sun W. 3D bioprinting of hepatoma cells and application with microfluidics for pharmacodynamic test of metuzumab. *Biofabrication*. 2019;11(3):034102.
doi: 10.1088/1758-5090/ab256c

26. McGuckin C, Forraz N, Milet C, et al. World's first long-term colorectal cancer model by 3D bioprinting as a mechanism for screening oncolytic viruses. *Cancers*. 2023;15(19):4724.
doi: 10.3390/cancers15194724

27. Prashantha K, Krishnappa A, Muthappa M. 3D bioprinting of gastrointestinal cancer models: a comprehensive review on processing, properties, and therapeutic implications. *Biointerphases*. 2023;18(2):020801.
doi: 10.1116/6.0002372

28. Sun H, Sun L, Ke X, et al. Prediction of clinical precision chemotherapy by patient-derived 3D bioprinting models of colorectal cancer and its liver metastases. *Adv Sci*. 2024;11(2):2304460.
doi: 10.1002/advs.202304460

29. Sun H, Wang Y, Yang H. Revolutionizing preclinical research for pancreatic cancer: the potential of 3D bioprinting technology for personalized therapy. *Hepatobiliary Surg Nutr*. 2023;12(4):616-618.
doi: 10.21037/hbsn-23-248

30. Li C, Jin B, Sun H, et al. Exploring the function of stromal cells in cholangiocarcinoma by three-dimensional bioprinting immune microenvironment model. *Front Immunol*. 2022;13:941289.
doi: 10.3389/fimmu.2022.941289

31. Yue K, Santiago GT de, Alvarez MM, Tamayol A, Annabi N, Khademhosseini A. Synthesis, properties, and biomedical applications of gelatin methacryloyl (GelMA) hydrogels. *Biomaterials*. 2015;73:254-271.
doi: 10.1016/j.biomaterials.2015.08.045

32. Nikkhah M, Eshak N, Zorlutuna P, et al. Directed endothelial cell morphogenesis in micropatterned gelatin methacrylate hydrogels. *Biomaterials*. 2012;33(35):9009-9018.
doi: 10.1016/j.biomaterials.2012.08.068

33. Kaemmerer E, Melchels FPW, Holzapfel BM, Meckel T, Hutmacher DW, Loessner D. Gelatine methacrylamide-based hydrogels: an alternative three-dimensional cancer cell culture system. *Acta Biomater*. 2014;10(6):2551-2562.
doi: 10.1016/j.actbio.2014.02.035

34. Bertassoni LE, Cardoso JC, Manoharan V, et al. Direct-write bioprinting of cell-laden methacrylated gelatin hydrogels. *Biofabrication*. 2014;6(2):024105.
doi: 10.1088/1758-5082/6/2/024105

35. Chen MB, Srigunapalan S, Wheeler AR, Simmons CA. A 3D microfluidic platform incorporating methacrylated gelatin hydrogels to study physiological cardiovascular cell-cell interactions. *Lab Chip*. 2013;13(13):2591-2598.
doi: 10.1039/c3lc00051f

36. Janisiewicz AM, Shin JH, Murillo-Sauca O, et al. CD44(+) cells have cancer stem cell-like properties in nasopharyngeal carcinoma. *Int Forum Allergy Rhinol*. 2012;2(6):465-470.
doi: 10.1002/alr.21068

37. Liu SX, Wang C, Lin RB, et al. Super-enhancer driven SOX2 promotes tumor formation by chromatin re-organization in nasopharyngeal carcinoma. *EBioMedicine*. 2023;98:104870.
doi: 10.1016/j.ebiom.2023.104870

38. Tang J, Zhong G, Wu J, Chen H, Jia Y. SOX2 recruits KLF4 to regulate nasopharyngeal carcinoma proliferation via PI3K/AKT signaling. *Oncogenesis*. 2018;7(8):61.
doi: 10.1038/s41389-018-0074-2

39. Chen L, Chiang YC, Chan LS, et al. The CBP/β-catenin antagonist, ICG-001, inhibits tumor metastasis via blocking of the miR-134/ITGB1 axis-mediated cell adhesion in nasopharyngeal carcinoma. *Cancers (Basel)*. 2022;14(13):3125.
doi: 10.3390/cancers14133125

40. Jin S, Li R, Chen MY, et al. Single-cell transcriptomic analysis defines the interplay between tumor cells, viral infection, and the microenvironment in nasopharyngeal carcinoma. *Cell Res*. 2020;30(11):950-965.
doi: 10.1038/s41422-020-00402-8

41. Sun L, Guo S, Xie Y, Yao Y. The characteristics and the multiple functions of integrin β1 in human cancers. *J Transl Med*. 2023;21(1):787.
doi: 10.1186/s12967-023-04696-1

42. Urien S, Lokiec F. Population pharmacokinetics of total and unbound plasma cisplatin in adult patients. *Br J Clin Pharmacol*. 2004;57(6):756-763.
doi: 10.1111/j.1365-2125.2004.02082.x

43. Joerger M, von Pawel J, Kraff S, et al. Open-label, randomized study of individualized, pharmacokinetically (PK)-guided dosing of paclitaxel combined with carboplatin or cisplatin in patients with advanced non-small-cell lung cancer (NSCLC). *Ann Oncol*. 2016;27(10):1895-1902.
doi: 10.1093/annonc/mdw290

44. Casale F, Canaparo R, Serpe L, et al. Plasma concentrations of 5-fluorouracil and its metabolites in colon cancer patients. *Pharmacol Res*. 2004;50(2):173-179. doi: 10.1016/j.phrs.2004.01.006

45. Bossi P, Chan AT, Licitra L, et al. Nasopharyngeal carcinoma: ESMO-EURACAN clinical practice guidelines for diagnosis, treatment and follow-up†. *Ann Oncol*. 2021;32(4):452-465. doi: 10.1016/j.annonc.2020.12.007

46. Chen YP, Yin JH, Li WF, et al. Single-cell transcriptomics reveals regulators underlying immune cell diversity and immune subtypes associated with prognosis in nasopharyngeal carcinoma. *Cell Res*. 2020;30(11):1024-1042. doi: 10.1038/s41422-020-0374-x

47. Tang XR, Li YQ, Liang SB, et al. Development and validation of a gene expression-based signature to predict distant metastasis in locoregionally advanced nasopharyngeal carcinoma: a retrospective, multicentre, cohort study. *Lancet Oncol*. 2018;19(3):382-393. doi: 10.1016/S1470-2045(18)30080-9

48. Weichselbaum RR, Ishwaran H, Yoon T, et al. An interferon-related gene signature for DNA damage resistance is a predictive marker for chemotherapy and radiation for breast cancer. *Proc Natl Acad Sci U S A*. 2008;105(47):18490-18495. doi: 10.1073/pnas.0809242105

49. Tan Z, Xiao L, Tang M, et al. Targeting CPT1A-mediated fatty acid oxidation sensitizes nasopharyngeal carcinoma to radiation therapy. *Theranostics*. 2018;8(9):2329-2347. doi: 10.7150/thno.21451

50. Sun Z, Wang X, Wang J, et al. Key radioresistance regulation models and marker genes identified by integrated transcriptome analysis in nasopharyngeal carcinoma. *Cancer Med*. 2021;10(20):7404-7417. doi: 10.1002/cam4.4228

51. Zhang B, Li J, Wang Y, et al. Deubiquitinase USP7 stabilizes KDM5B and promotes tumor progression and cisplatin resistance in nasopharyngeal carcinoma through the ZBTB16/TOP2A axis. *Cell Death Differ*. 2024;31(3):309-321. doi: 10.1038/s41418-024-01257-x